Detection of Ethanol Concentration in Liquid Using a Double Layered Resonator Operating at 5g Mm-wave Frequencies

Suhail Asghar Qureshi
Universiti Tun Hussein Onn Malaysia
Zuhairiah Zainal Abidin (zuhairia@uthm.edu.my)
Universiti Tun Hussein Onn Malaysia https://orcid.org/0000-0002-7774-6703
Huda A. Majid
Universiti Tun Hussein Onn Malaysia
Adel YI Ashyap
Universiti Tun Hussein Onn Malaysia
Chan Hwang See
Edinburgh Napier University

Research Article

Keywords: Resonator, 5G mm-wave, ethanol, liquid, sensor

Posted Date: April 11th, 2022

DOI: https://doi.org/10.21203/rs.3.rs-1529116/v1

Abstract

This paper discusses a new sensing technique for detecting ethanol concentration in aqueous solutions rapidly based on electromagnetic resonance. The sensor consists of two substrate layers and operates at 5G millimetre-wave frequencies (5G mm-wave). An experimental study of the new resonator's configuration is undertaken in determining the sensor's sensitivity. During the measurements, 6 samples were modelled with varying amounts of ethanol concentration in the water. The results showed that S_{11} resonance moves linearly towards higher frequencies as the ethanol content increases. The resonance shifted by 178 MHz for every 10% increase in ethanol. As a result, the proposed 5G mm-Wave sensing technique based on a replaceable sensing layer proves to be suitable for rapid, accurate, and low-cost alcohol content detection in liquids.

1. Introduction

The perseverance of the ethanol content of alcohol is critical for quality control during the manufacturing process. Specific regulatory guidelines must be followed during the final stages of the brewing process of alcoholic beverages. Alcohol beverages can be prohibitively expensive in developing countries. As a result, consumers demand lower-priced goods. Under such circumstances, merchants can illegally add ethanol to the beverage to increase its alcohol content and thus lower its price.[1] According to one study, the ethanol content of red vine can range between 8% and 15% by volume.[2] Nonetheless, drinking alcohol with a high ethanol content can produce formic acid, which can cause various health problems, including fatigue, vertigo, blurred vision, and vomiting, as well as death.[3,4] As a result, it is necessary to develop a mechanism for monitoring these beverages' ethanol content using rapid testing to avoid potential health risks.

Traditional optical refraction-based methods are used to determine the quality of alcohol. However, the sugar content has an inescapable effect on the measurements [5] and a hydrometer is typically required to determine the specific gravity of a liquid during an examination. To improve the accuracy of the measurement, two advanced optical techniques, i.e. Raman spectroscopy and infrared wavelengths are proposed.[6] They are, however, susceptible to carbonation and fluorescence. Additionally, it is difficult to disentangle the contributions of ethanol and sugar from spectral signature.[5] Numerous approaches and techniques are being used to fabricate viable, affordable, and portable sensors.[7] Due to the robustness, low cost, and high sensitivity of microwave sensors, this technology is more advanced in the chemical and biomedical fields than traditional sensing methods.[8]

In general, resonators used in sensing or measuring equipment provide precise measurements of the electromagnetic properties of any material at microwave frequencies. For low-loss materials, the resonant method provides accurate measurements. Resonators are well-known for their compact size, low sample volume requirement, and sharp reflection/transmission coefficient representation, which results in enhanced performance.[9] Additionally, this enables them to be used as instruments for measuring a

variety of physical parameters dependent on the permittivity or permeability of the sample.[10] According to the measured physical parameters, microwave resonators are configured to produce a relative resonant frequency and/or oscillating phase response.[11]

In Reference[12], a resonator sensor was demonstrated for ethanol, methanol, and isopropyl alcohol (IPA) applications. The chiral metamaterial structure based on three unit cells demonstrated a sensing frequency range of 280 MHz for measurements of IPA-water solutions containing 10–90% IPA.[12] Additionally, resonating structures incorporating transmission lines have been reported for use in various sensory applications.[13–15] In Reference[16], a contactless sensor operating at 2.4 GHz was used to characterise liquids. The material under test (MUT) was inserted inside a capillary tube parallel to the sensor's surface and the transmission coefficient (S_{21}) shift was observed. The analysis was conducted by establishing a reference sample and correlating it to other samples.[16] The same phenomenon was demonstrated in Rererence[13], where a pair of split-ring resonators was used to identify various loads using the transmission coefficient as the primary sensing parameter. In Rererence[14], an omega-shaped resonator coupled to a microstrip transmission line was proposed for analysing changes in Q-factor and S_{21} as a function of chemical content variation in oil. Additionally, measurements in the frequency range of 2.5 GHz to 3 GHz were made on ethanol and methanol mixtures with pure water.[14] Another transmission line sensor for characterising methanol was proposed in Reference.[17] The measurements were made between 6 and 8 GHz. The resonant frequency shift was monitored up to 0.15 GHz for methanol concentrations ranging from 0 to 100%.[17] However, to the author's knowledge, no resonator for the characterisation of alcohol liquids that operates at higher frequencies, such as 5G millimetre-wave (mm-wave) frequencies, has been proposed.

It is worth noting that liquids with high water content, such as alcohol and other aqueous solutions, are dispersive media with frequency-dependent electromagnetic properties. The mm-wave frequency range is well suited for alcohol sensing because it increases sensitivity to the analyte sample's dielectric constant and loss tangent.[18] Additionally, switching from lower microwave frequencies to this frequency results in a reduction in the size of the resonators while increasing the spatial resolution of the designed sensors.[19] Taking these advantages of mm-wave frequencies into account, we propose a double-layered resonator for detecting the presence of ethanol in liquid solutions at 5G mm-wave frequencies. Recently, several microwave sensing techniques have been proposed, including microfluidic channels,[20] the substrate-etched method,[14,21] and the use of a sample holder/case.[22] They are, however, challenging to integrate into practical applications and may necessitate a large sample volume for examination. Additionally, it is challenging to completely purify the sample holder or microfluidic channel following each measurement. As a result, the proposed sensor comprises two substrate layers, the top layer of which can be easily replaced between measurements.

2. Design And Fabrication Of The Sensor

The CST microwave studio was used to design the double-layered microwave sensor, and the Finite Integration Technique (FIT) was used to simulate it in the frequency range of 20 GHz to 35 GHz. As illustrated in Fig. 1, the sensor comprises two layers of Rogers RT/Duroid 5880 material with a dielectric constant of 2.2 and a loss tangent of 0.0009. The proposed integrated sensor can be physically formed by stacking the top and bottom layers. The sensor design utilises a substrate with a thickness of 1.57 mm for the bottom layer and 0.127 mm for the top layer. As illustrated in Fig. 1a, the bottom substrate layer contains a couple of transmission lines that are connected via ports P1 (Port 1) and P2 (Port 2). The top layer positioned directly above the transmission line layer's centre consists of a resonator with a couple of triangular and rectangular enclosing both triangular (Fig. 1b). As illustrated in Fig. 1c, a copper sheet with a thickness of 35 nm completely covers the backside of the bottom substrate layer, which serves as the ground plane. There is no ground between the transmission line and the top substrate layer, allowing for maximum coupling between the two layers.

The dimensions of the resonating structure are represented in Table I. The resonator design was fabricated by transforming the analytical model of CST into the physical structure. The fabricated design is shown in Fig. 2, connected by two 2.4 mm reusable SMA connectors. The magnitude of the reflection coefficient of the sensor design can be mathematically defined by Eq. 1.[23]

Table I. Optimised dimensions of sensor

Dimension	Value (mm)
L_2	6.0
T_0	3.1
W	0.6
L_1	4.60

$$S_{11} = 20\log\left|\frac{Z_{in} - Z_0}{Z_s - Z_0}\right| \quad (1)$$

where Z_{in} is the input impedance realised at port 1 (P1), while Z_0 is characteristics impedance of the transmission line on the bottom substrate layer. Z_s on other hand, is defined by Eq. 2.[23]

$$Z_s\left(\omega, \epsilon_{eff}\right) = j\omega L + j\omega^3 \times \left(\frac{C_s\left(\epsilon_{eff}\right) M^2 \times \left(1 - \frac{\omega^2}{\omega_0^2}\right) + 2\omega^2 M^2 M' C_s\left(\omega_{eff}\right)^2}{\left(1 - \frac{\omega^2}{\omega_0^2}\right) - \omega^4 M'^2 C_s\left(\omega_{eff}\right)^2} \right)$$

2

Resonators typically have the resonance that can be electrically modelled using the lumped elements, C_{eff}, L_{eff} and R. L_{eff} is the resonating structure's equivalent inductance. The equivalent circuit of the designed resonator is depicted in Fig. 3. The inductance of the design consists of two parts; (i) mutual inductance between adjacent triangular resonator (M), and (ii) mutual inductance between two adjacent slots (M'), eventually forming a rectangular. C_{eff} is defined as the equivalent capacitance of the entire structure, including the capacitances produced between the triangular resonators and the adjacent slots. By adding the triangular resonators between the two slots, the effective capacitance can be increased, which improves the interaction between the resonating structure and the sample. By modifying the sample within the proximity of the sensor, the effective permittivity of the sensor will be changed.

Consequently, variation in effective permittivity, ϵ_{eff} will change the overall capacitance, C_S, thereby changing the input impedance realised at port 1 (P1). The effective resistance is defined by R, which depends on the conductivity of copper material and the sample. ω^0 represents the resonant frequency of the structure. This model aims to show the implicit association of the reflection coefficient and the sensing method of the sensor. This relationship will help to understand the effect of the sample's permittivity variation in the following sections of this paper. The comparison of the simulated and measured reflection coefficient (S_{11}) behaviour is shown in Fig. 4, where the design is found to be resonating at 27.575 GHz with a negative amplitude of 47 dB. It is authenticated that the simulated and measured results are in good agreement at the resonant frequency. However, slight variations in amplitude can occur due to environmental parameters and imperfect fabrication.

3. Results And Analysis

A. Sample's Permittivity Analysis

It is required to know the effective permittivity and tangent loss of samples at the operating frequency range. Therefore, it is essential to determine the complex dielectric permittivity of the LUTs (Liquid Under Test) used during measurements. The dispersive permittivity characteristics of the samples in complex form can be expressed using Eq. 3:

$$\epsilon_r(f) = \epsilon_r'(f) - \epsilon_r''(f)$$

3

In Eq. 3, $\epsilon_r^{'}$ is real permittivity, $\epsilon_r^{''}$ is imaginary permittivity while f is the frequency that defines the dispersive characteristics over the operating range of frequencies (20–35 GHz). The instantaneous permittivity over the operating frequency range is measured because materials' permittivity exhibit a frequency dispersive phenomenon at high frequencies.[19] The electromagnetic response of microwaves with water is considered a good starting point for developing a sensor because water is major content in alcohol.[24] In this study, we chose ethanol as the LUT that is divided into 6 values of concentration ranging from 0 to 90% obtained by adding 0, 17.5 ml, 22.5 ml, 35 ml, 40 ml and 45 ml ethanol into 50 ml, 32.5 ml, 27.5 ml, 15 ml, 10 ml and 5 ml of water, respectively. According to extensive research, water has a higher permittivity than alcohol.[25,26] The permittivity of the LUTs was measured using the Keysight 85070E Dielectric Probe Kit, which can be expressed in terms of the fitted Debye parameters. The Debye model is defined by Eq. 4:

$$\epsilon = \epsilon_\infty + \frac{\epsilon_s - \epsilon_\infty}{1 + j\omega\tau}$$

4

where ϵ_∞ is the dielectric constant at high frequencies, ϵ_s is the dielectric constant at low frequencies and τ is relaxation time constant. The fitted parameters of the Debye model for each sample used in measurements are given in Table II.

Table II. Composition of liquid samples

Ethanol (%)	90	80	70	45	35	0
ϵ_∞	1.44	1.5	1.62	1.85	2.29	7.73
ϵ_s	10.85	24.2	44.05	61.51	71.17	78.36
τ (ps)	22.5	33.86	47.8	32.85	24.45	8.92

B. Simulation analysis of ethanol with different concentrations

During the simulations, the samples (LUTs) were modelled by loading the permittivity values obtained in Section 3A. As illustrated in Fig. 5, the LUT was loaded across the sensor's surface, completely covering the resonator structure. Each sample's resonant frequency was determined by substituting its dielectric properties. The transmission parameter, e.g. S_{21}, is typically taken into account to determine the resonant frequency. This parameter corresponds to the signal's negative peak. Notably, our design had a negative peak in S_{11} rather than S_{21}, which is consistent with previously described sensors with S_{11} as the sensing parameter.[12,23,27,28] Fig. 6 illustrates the simulated resonant frequencies for various ethanol

concentrations. The resonant frequencies of samples at concentrations of 90%, 80%, 70%, 45.5%, 35.5%, and 0% are 27.06 GHz, 26.98 GHz, 26.9 GHz, 26.68 GHz, 26.58 GHz, and 26.34 GHz, respectively.

It is demonstrated that as the ethanol concentration increases, the resonant frequency moves toward higher frequencies. It is worth noting that the difference between the first and second data points (0 and 35% ethanol) is more significant than the difference between the other intervals, owing to the more significant difference in their permittivity levels as defined by the Debye parameters in Table II. This introduces a small amount of non-linearity into the intervals, as the difference in resonant frequencies between samples containing 70 and 80 per cent ethanol and samples containing 80 and 90% ethanol is only 0.08 GHz.

Additionally, the linear regression analysis was used to determine the sensor's resonance shift in response to changes in ethanol concentration. This application seeks to establish a relationship between the input (ethanol concentration) and the output (resonant frequency). After establishing a functional relationship between these two variables using training data on obtained results, the relationship is validated using the same linear regression method on data that was not used during training. Thus, the validated model can be used to forecast the output when the input data is unknown.[29] The output of regression analysis applied to the resonance shift is shown in Fig. 6, where R^2 is the coefficient of determination. The coefficient of determination indicates the degree to which the model fits accurately. It has a value between 0 and 1 and indicates the number of data points, which lie on the regression line. The obtained R^2 value of 0.9966 indicates that a significant proportion of data points lie on the regression line, implying that unknown outputs can be predicted with reasonable accuracy.

C. Experimental analysis of ethanol with different concentrations

During the measurements, coaxial cables from the N5234B PNA-L Vector Network Analyzer (VNA) were connected to the sensor's transmission lines via 2.4 mm reusable SMA connectors, as shown in Fig. 7. Before performing the measurements, the VNA was calibrated in three stages in the desired frequency range (20–35 GHz): open circuit, short circuit, and 50 loads. The same six liquid samples listed in Table II were prepared with ethanol concentrations ranging from 0–90% to avoid unnecessary complexity. The dropper was used to insert liquid over the sensor’s surface covering the entire resonator structure. The shift in resonance caused by adding alcohol to water is depicted in Fig. 8. Understandably, as the concentration of ethanol increases, the resonant frequency increases that is consistent with the simulated results. The resonant frequencies for samples containing 90% ethanol and 0% ethanol are 27.05 GHz and 25.55 GHz, respectively, while the resonant frequencies for samples containing 80%, 45%, 35%, and 0% ethanol are 26.68 GHz, 26.6 GHz, 26.3 GHz, and 26.15 GHz, respectively. When applying regression analysis on the data points, measured results show a coefficient of determination of R^2 = 0.978, which is slightly less than the simulated result. The obtained coefficient of determination is still a significant number implying that the higher percentage of data points in measurements lie on the regression line.

The electric energy stored at the resonance frequency must equal the magnetic field stored in the resonating structure. The presence of an external field influences the net electric and magnetic fields, consequently causing a disturbance in the resonance. Eq. 5 can be used to get insight into the variation in dielectric properties of the external disturbances by associating permittivity and permeability of the external medium with the resonant frequency's perturbation.[30] Perturbation is the phenomenon of realising change in quality factor and/or shift in resonant frequency.[31]

$$\frac{\Delta f_r}{f_r} = \frac{\int_0^v \left(\Delta \epsilon E_0 E_1 + \Delta \mu H_0 H_1 \right) dv}{\int_0^v \left(\epsilon_0 \left| E_0 \right|^2 + \left| H_0 \right|^2 \mu_0 \right) dv}$$

5

where v represents the volume of external medium that is the volume of a sample that interacts with the EM fields of the structure; E_0 and H_0 are electric field distributions and magnetic field distributions without external distributions, respectively; ϵ_0 and μ_0 are permittivity and permeability of free space, respectively; The change in the resonance (quality factor and/or shift) is represented by Δf; change in net permittivity and permeability with an external medium is represented by $\Delta \epsilon$ and $\Delta \mu$, respectively; and E_1 represents the external fields' electric field distribution and H_1 represents external fields' magnetic field distribution.

As stated in Section 2, the external medium's permittivity adds to the effective capacitance (C_{eff}) from FTL's one side to the other side and its permeability adds to the induced current in the resonant element. Thus, it is reaffirmed that the permittivity of the introduced medium strongly influences the resonator structure on the top layer. Since the original fields have incorporated the aqueous solutions used in this work, it cannot be expected that the resonator's internal field patterns will be approximately equal to the resonator's field patterns without samples. It is because the interval field patterns show complicated field distributions after the placement of the sample. Even though the accurate prediction of the relationship is not possible, resonance shift can be realised versus ethanol's concentration by a change in their permittivity values. From Eq. 6, the relative perturbation in the reflection coefficient can be approximated as [32]:

$$\frac{\Delta f_r}{f_r} \approx \frac{-|\Delta \epsilon| h}{2|\epsilon| L}$$

6

where $\Delta \epsilon$ is the difference in the permittivity of two consecutive ethanol concentrations as listed in Table II, f_r is the reference resonant frequency, Δf_r is the difference between reference and next resonant

frequency, h is the height of the sample's drop introduced on the sensor's surface, while L is the length of the sample's drop.

According to the measured results, the average $\frac{\Delta f_r}{f_r}$ for 10% change in ethanol's concentration is determined as 0.178. The average length and its height of drop introduced on the sensor's surface covering resonator structure entirely was 8 mm and 1 mm, respectively. Thus, the calculated average $\frac{\Delta f_r}{f_r}$ using Eq. 6 per 10% change in ethanol's concentration, 0.146 is comparatively in agreement with measured results, which validates the application of the proposed geometry.

4. Discussion

The simulation results showed a total resonance shift in S_{11} of up to 0.72 GHz as ethanol concentration in aqueous solutions varied. On the other hand, the measurements revealed a 0.9 GHz shift in the S_{11} resonance frequency as the ethanol concentration increased from 0–90%. The simulated and measured reflection coefficients in the case of each sample are demonstrated in Fig. 9. The minor disparity in these results is due to the simulation tool's inability to match physical parameters such as sample volume and temperature during measurements. Additionally, measurements on the fabricated sensor demonstrate a resonance shift of up to 0.128 GHz per 10% change in ethanol concentration.

The measured sensitivity in this study is compared to the previously proposed state-of-the-art resonator-based liquid sensors in Table III. It should be noted that the solute used in the measurements may also affect the resonance due to the difference in permittivity between it and the solvent. For example, some studies employed liquid samples other than alcohols, but their sensitivity is low,[12,32,33] except for a study conducted by Bakir et al.,[12] in which kerosene was used as the solute. Due to the strong chiral electromagnetic fields present in the chiral structure.[12] In comparison, studies using alcohol samples revealed a very low sensitivity, owing to the lower frequency of operation. We used ethanol as the solute in our study, and the sensor demonstrated the most significant shift in resonance for various ethanol concentrations compared to previously studied structures. Following the sensitivity comparison, it can be reiterated that the use of 5G mm-wave frequencies results in an increase in the perturbation of S-parameters in response to liquid permittivity variations.

Table III. State-of-art liquid resonator-based liquid sensors

Reference	Solute	Operating frequency	Sensitivity (Δf/10%)
27	Ethanol	0.225 GHz	0.0042 GHz
17	Methanol	6.5 GHz	0.015 GHz
32	Saline	11.6 GHz	0.026 GHz
34	Isopropanol	5.4 GHz	0.03 GHz
35	Ethanol	2.15 GHz	0.034 GHz
14	Methanol	2.7 GHz	0.062 GHz
33	Magnesium sulphate	2 GHz	0.0784 GHz
36	Ethanol	5.5 GHz	0.085 GHz
37	Ethanol	4 GHz	0.095 GHz
12	Kerosene	9.8 GHz	0.16 GHz
This work	Ethanol	27.57 GHz	0.178 GHz

5. Conclusion

The article discusses a novel microwave sensing technique featuring a replaceable resonator-based sensing layer for repeatable measurement without any need of disconnecting the sensor from VNA. Two layers comprise the sensor: a substrate for the transmission line that connects to the VNA and a sensing layer with a resonator structure. The design was modelled and simulated in the 20–35 GHz frequency range. The sensor was constructed and tested to determine its performance in detecting the presence of ethanol in a liquid. A change in the concentration of ethanol in aqueous solutions changes the input impedance of the resonator's transmission line, which consequently influences the reflection coefficient. Thus, the change in ethanol concentrations attains S_{11} perturbation. Experiments with water-alcohol solutions were conducted to analyse the sensor's performance. Due to the sensor's transition to a higher frequency, it demonstrated higher sensitivity up to 178 MHz as the ethanol concentration in the liquid increased by 10% in volume than the sensors operating at lower frequencies. Due to the lack of control over the sample volume, a small discrepancy between the simulated and measured results was observed. The results of the experiments indicate that the sensor operating in the 5G mm-wave band is susceptible to lossy liquids, as demonstrated by the concentrations of water and alcohol.

Declarations

Acknowledgement

This study was funded by Ministry of Higher Education (MoHE) Malaysia under Fundamental Research Grant Scheme Vot No. FRGS/1/2019/TK04/UTHM/02/13, and it is partially sponsored by Universiti Tun Hussein Onn Malaysia (UTHM).

Conflict of interest

The authors declare that they have no conflict of interest.

References

1. S.K. Tulashie, A.P. Appiah, G.D. Torku, A.Y. Darko, A. Wiredu, Determination of methanol and ethanol concentrations in local and foreign alcoholic drinks and food products (Banku, Ga kenkey, Fante kenkey and Hausa koko) in Ghana. Int. J. Food Contam. **4**(1), 14 (2017). doi:10.1186/s40550-017-0059-5
2. A. Cordova, B. Sumpio, Polyphenols are medicine: Is it time to prescribe red wine for our patients? Int. J. Angiol. **18**(03), 111–117 (2009). doi:10.1055/s-0031-1278336
3. C. Md, T. Elena, F. Ibolya, F. Erzsébet, A Survey on the Methanol Content of Home Distilled Alcoholic Beverages in Transylvania (Romania). Acta Med. Marisiensis **59**(4), 206–208 (2013). doi:10.2478/amma-2013-0048
4. E.I. Ohimain, Methanol contamination in traditionally fermented alcoholic beverages: the microbial dimension. Springerplus **5**(1), 1607 (2016). doi:10.1186/s40064-016-3303-1
5. K. Bertling, S. Han, T. Wu, C. Zhao, Y.L. Lim, P. Dean, S.P. Khanna, D. Indjin, E.H. Linfield, A.G. Davies, S.J. Wilson, Determining Ethanol Content of Liquid Solutions Using Laser Feedback Interferometry with a Terahertz Quantum Cascade Laser. IEEE Sens. Lett **2**(3), 1–4 (2018). doi:10.1109/LSENS.2018.2858927
6. K. De Wilder, G. De Roeck, L. Vandewalle, The Use of Advanced Optical Measurement Methods for the Mechanical Analysis of Shear Deficient Prestressed Concrete Members. Int. J. Concr Struct. Mater. **10**(2), 189–203 (2016). doi:10.1007/s40069-016-0135-x
7. E. Ekmekci, U. Kose, A. Cinar, O. Ertan, Z. Ekmekci, The use of metamaterial type double-sided resonator structures in humidity and concentration sensing applications. Sens. Actuators Phys **297**, 111559 (2019). doi:10.1016/j.sna.2019.111559
8. C. Zebiri, W. Mshwat, J. Kosha, M. Lashab, I. Elfergani, D. Sayad, S. Mosbah, J. Rodreguez, Y. AlYasir, R.A. Abd-Alhameed, A Metamaterial-Based Microwave Sensor for Liquid Dielectrics Characterization. PervasiveHealth Pervasive Comput Technol Healthc **2**, 97–106 (2020). doi:10.4108/eai.28-6-2020.2297951
9. A. Verma, S. Bhushan, P.N. Tripathi, M. Goswami, B.R. Singh, A defected ground split ring resonator for an ultra-fast, selective sensing of glucose content in blood plasma. J. Electromagn. Waves Appl. **31**(10), 1049–1061 (2017). doi:10.1080/09205071.2017.1325011

10. J. Mazierska, J. Krupka, M. Bialkowski, M.V. Jacob. Microwave resonators and their use as measurement instruments and sensors. In: *Third IEEE International Workshop on Electronic Design, Test and Applications (DELTA'06)*. IEEE; 2006:5 pp. – 167. doi:10.1109/DELTA.2006.67
11. R.M. Langdon, Resonator sensors-a review. J. Phys. E **18**(2), 103–115 (1985). doi:10.1088/0022-3735/18/2/002
12. M. Bakır, M. Karaaslan, E. Unal, F. Karadag, F. Alkurt, O. Altıntaş, S. Dalgac, C. Sabah, Microfluidic and Fuel Adulteration Sensing by Using Chiral Metamaterial Sensor. J. Electrochem. Soc. **165**(11), B475–B483 (2018). doi:10.1149/2.0231811jes
13. A. Ebrahimi, J. Scott, K. Ghorbani, Differential sensors using microstrip lines loaded with two split-ring resonators. IEEE Sens. J. **18**(14), 5786–5793 (2018). doi:10.1109/JSEN.2018.2840691
14. Y.I. Abdulkarim, L. Deng, M. Karaaslan, O. Altıntaş, H.N. Awl, F.F. Muhammadsharif, C. Liao, E. Unal, H. Luo, Novel Metamaterials-Based Hypersensitized Liquid Sensor Integrating Omega-Shaped Resonator with Microstrip Transmission Line. Sensors **20**(3), 943 (2020). doi:10.3390/s20030943
15. Y.I. Abdulkarim, L. Deng, M. Karaaslan, Ş Dalgaç, R.H. Mahmud, F. Ozkan Alkurt, F.F. Muhammadsharif, H.N. Awl, S. Huang, H. Luo, The Detection of Chemical Materials with a Metamaterial-Based Sensor Incorporating Oval Wing Resonators. Electronics **9**(5), 825 (2020). doi:10.3390/electronics9050825
16. E.L. Chuma, Y. Iano, G. Fontgalland, L.L. Bravo Roger, Microwave sensor for liquid dielectric characterization based on metamaterial complementary split ring resonator. IEEE Sens. J. Published online (2018). doi:10.1109/JSEN.2018.2872859
17. S. Dalgac, V. Akdogan, S. Kiris, A. Incesu, O. Akgol, E. Unal, M.T. Basar, M. Karaaslan, Investigation of methanol contaminated local spirit using metamaterial based transmission line sensor. Measurement **178**, 109360 (2021). doi:10.1016/j.measurement.2021.109360
18. A.E. Omer, S. Safavi-Naeini, R. Hughson, G. Shaker, Blood Glucose Level Monitoring Using an FMCW Millimeter-Wave Radar Sensor. Remote Sens. **12**(3), 385 (2020). doi:10.3390/rs12030385
19. A. Molaei, J. Heredia-Juesas, G. Ghazi, J. Vlahakis, J.A. Martinez-Lorenzo, Digitized Metamaterial Absorber-Based Compressive Reflector Antenna for High Sensing Capacity Imaging. IEEE Access. **7**, 1160–1173 (2019). doi:10.1109/ACCESS.2018.2881103
20. P. Velez, J. Munoz-Enano, K. Grenier, J. Mata-Contreras, D. Dubuc, F. Martin, Split Ring Resonator-Based Microwave Fluidic Sensors for Electrolyte Concentration Measurements. IEEE Sens. J. **19**(7), 2562–2569 (2019). doi:10.1109/JSEN.2018.2890089
21. Ş Dalgaç, M. Furat, M. Karaaslan, O. Akgöl, F. Karadağ, M. Zile, M. Bakir, Grease oil humidity sensor by using metamaterial. J. Electromagn. Waves Appl. **34**(18), 2488–2498 (2020). doi:10.1080/09205071.2020.1824690
22. A.E. Omer, G. Shaker, S. Safavi-Naeini, K. Ngo, R.M. Shubair, G. Alquié, F. Deshours, H. Kokabi, Multiple-Cell Microfluidic Dielectric Resonator for Liquid Sensing Applications. IEEE Sens. J. **21**(5), 6094–6104 (2021). doi:10.1109/JSEN.2020.3041700

23. M.A. Zidane, A. Rouane, C. Hamouda, H. Amar, Hyper-sensitive microwave sensor based on split ring resonator (SRR) for glucose measurement in water. Sens. Actuators Phys **321**, 112601 (2021). doi:10.1016/j.sna.2021.112601
24. S. Guha, F.I. Jamal, C. Wenger, A Review on Passive and Integrated Near-Field Microwave Biosensors. Biosensors **7**(4), 42 (2017). doi:10.3390/bios7040042
25. Z.O. Rodríguez-Moré, H. Lobato-Morales, R.A. Chávez-Pérez, J.L. Medina-Monroy, Complex dielectric permittivity of rum and its mixtures with methanol, ethanol, and water at frequencies up to 15 GHz. J. Microw. Power Electromagn. Energy **52**(1), 16–30 (2018). doi:10.1080/08327823.2017.1421013
26. R. Augustine, S. Raman, A. Rydberg, Relative permittivity measurements of Et–OH and Mt–OH mixtures for calibration standards in 1–15 GHz range. Electron. Lett. **50**(5), 358–359 (2014). doi:10.1049/el.2013.4300
27. C.-S. Lee, B. Bai, Q.-R. Song, Z.-Q. Wang, G.-F. Li, Open Complementary Split-Ring Resonator Sensor for Dropping-Based Liquid Dielectric Characterization. IEEE Sens. J. **19**(24), 11880–11890 (2019). doi:10.1109/JSEN.2019.2938184
28. T.G. Kang, J.K. Park, B.H. Kim, J.J. Lee, H.H. Choi, H.J. Lee, J.G. Yook, Microwave characterization of conducting polymer PEDOT: PSS film using a microstrip line for humidity sensor application. Measurement **137**, 272–277 (2019). doi:10.1016/j.measurement.2019.01.032
29. P. Rapp, M. Mesch, H. Giessen, C. Tarín, Regression Methods for Ophthalmic Glucose Sensing Using Metamaterials. J. Electr. Comput. Eng. **2011**, 1–12 (2011). doi:10.1155/2011/953064
30. J.G.D. Oliveira, E.N.M.G. Pinto, V.P.S. Neto, A.G. D'assunção. CSRR-based microwave sensor for dielectric materials characterization applied to soil water content determination. Sens. (Switzerland). 2020;20(1). doi:10.3390/s20010255
31. H. Lobato-Morales, D.V.B. Murthy, A. Corona-Chávez, J.L. Olvera-Cervantes, J. Martínez-Brito, L.G. Guerrero-Ojeda. Permittivity measurements at microwave frequencies using epsilon-near-zero (ENZ) tunnel structure. *IEEE Trans Microw Theory Tech*. Published online 2011. doi:10.1109/TMTT.2011.2132141
32. Y.J. Mao, Y.J. Zhang, Z.R. Chen, M.S. Tong, A Noncontact Microwave Sensor Based on Cylindrical Resonator for Detecting Concentration of Liquid Solutions. IEEE Sens. J. **21**(2), 1208–1214 (2021). doi:10.1109/JSEN.2020.3016290
33. R. Avalos Ribas, I.E. Gelosi, A.J. Uriz, J.C. Moreira, J.C. Bonadero, A High-Sensitivity Cylindrical Cavity Resonator Sensor for the Characterization of Aqueous Solutions. IEEE Sens. J. **21**(6), 7581–7589 (2021). doi:10.1109/JSEN.2020.3044859
34. J. Kilpijärvi, N. Halonen, J. Juuti, J. Hannu, Microfluidic Microwave Sensor for Detecting Saline in Biological Range. Sensors **19**(4), 819 (2019). doi:10.3390/s19040819
35. O. Altıntaş, M. Aksoy, E. Ünal, M. Karaaslan, C. Sabah, Operating Frequency Reconfiguration Study for a Split Ring Resonator Based Microfluidic Sensor. J. Electrochem. Soc. **167**(14), 147512 (2020). doi:10.1149/1945-7111/abc656

36. S. Kiani, P. Rezaei, M. Navaei, Dual-sensing and dual-frequency microwave SRR sensor for liquid samples permittivity detection. Measurement **160**, 107805 (2020). doi:10.1016/j.measurement.2020.107805
37. A. Karatepe, O. Akgöl, Y.I. Abdulkarim, Ş Dalgac, F.F. Muhammadsharif, H.N. Awl, L. Deng, E. Ünal, M. Karaaslan, L. Heng, S. Huang. Multipurpose chemical liquid sensing applications by microwave approach. Mukherjee K, ed. *PLoS One*. 2020;15(5):e0232460. doi:10.1371/journal.pone.0232460

Figures

Figure 1

Sensor design: (a) transmission line on the bottom layer, (b) resonator structure on the top layer, (c) side view of the integrated top and bottom layers and (d) 3D view

Figure 2

Fabricated design of the sensor

Figure 3

Equivalent circuit of the resonator

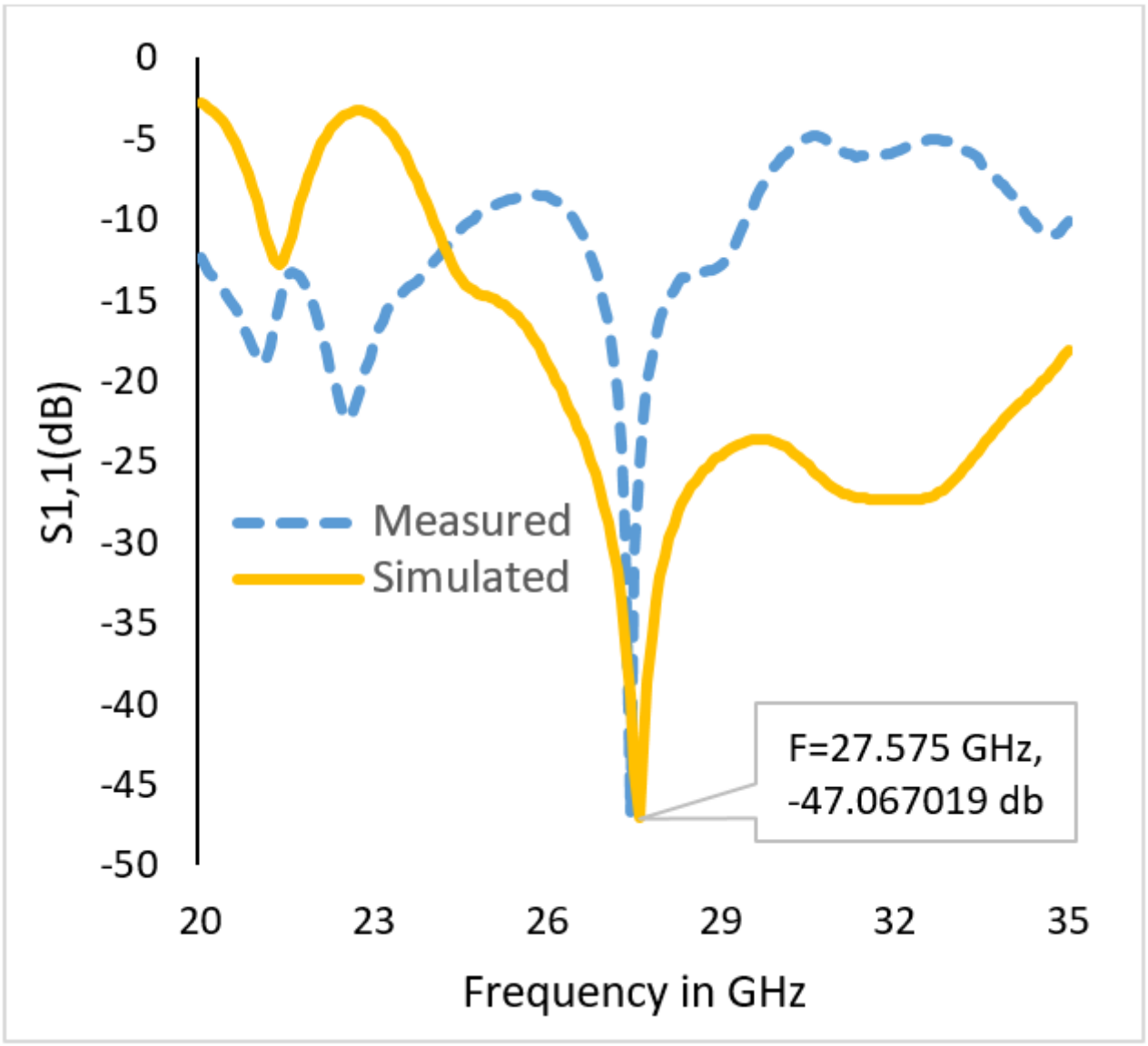

Figure 4

The resonant frequency of the sensor

Figure 5

Sample placement over the sensor's surface

Figure 6

Relationship of simulated resonant frequencies with ethanol concentration

Figure 7

Measurement setup

Figure 8

Relationship of measured resonant frequencies with ethanol concentration

Figure 9

Perturbation in reflection coefficient, S_{11} on varying ethanol concentration